ELSEVIER

Materials Science and Engineering A258 (1998) 75–83

MATERIALS SCIENCE & ENGINEERING A

Room temperature tensile properties of Fe–Al single crystals strengthened by excess vacancies

K. Yoshimi[a,*], Y. Saeki[1b], M.H. Yoo[c], S. Hanada[a]

[a] *Institute for Materials Research, Tohoku University, Sendai, 980-77, Japan*
[b] *Graduate Student, Department of Materials Processing, Tohoku University, Sendai, 980-77, Japan*
[c] *Metals and Ceramics Division, Oak Ridge National Laboratory, Oak Ridge, TN 37831-6115, USA*

Abstract

Effects of supersaturated excess vacancies on plastic deformation of Fe–Al were investigated by tensile testing at room temperature for three different single crystals (Fe-33, 41 and 44 mol% Al). Critical resolved shear stresses (CRSSs) of slowly-cooled specimens (as homogenized specimens) and well-annealed specimens (vacancy-eliminated specimens) were almost the same and did not show Al concentration dependence. On the other hand, the CRSS of vacancy-containing specimens (fast-cooled specimens) was significantly higher than that of the others, even for Fe-33 mol% Al, and showed strong Al concentration dependence. The fast-cooled specimens displayed serrated flow behavior during work-hardening at room temperature, and the serrated flow was more intensive at a higher Al composition. Deformation microstructures of Fe-44 mol% Al were examined by TEM, and it was found that dislocations in fast-cooled specimens were inhomogeneously distributed, suggesting jerky motion of slip dislocations. These dislocations were oriented along an unstable direction estimated from dislocation line tension. In addition, there were numerous dislocation loops. A dislocation mechanism of the excess vacancy strengthening is discussed on the basis of the experimental results. © 1998 Elsevier Science S.A. All rights reserved.

1. Introduction

It is well-known that excess vacancy strengthening is significant at low temperatures in Fe–Al, particularly in B2 FeAl. Special attention has been paid to this phenomenon since Nagpal and Baker reported the composition and cooling rate dependence of hardness in B2 FeAl [1]. This phenomenon was first reported by Rieu and Goux [2]. They revealed that B2 FeAl quenched rapidly from elevated temperatures retains a high concentration of thermal vacancies, and that the retained excess vacancies enhance hardness [2]. Since the excess vacancy concentration increases with increasing Al concentration, the strength of the iron aluminides exhibits strong composition dependence, if samples are subjected to the same thermal histories [1,3–5]. Furthermore it has been found that there is a linear relationship between the hardness and the square root of vacancy concentration [4].

One of the remaining problems is how Fe–Al is strengthened by excess vacancies. Kimura and Maddin [6] reviewed vacancy strengthening in fcc metals and considered that the strengthening is caused by the interaction of dislocations with 'observable vacancy clusters' and by super-jog formation due to condensation of vacancies on dislocations. In the case of B2 FeAl, however, the excess vacancy strengthening is likely to occur by mechanism(s) different from that in fcc metals, because: (1) Fe–Al does not exhibit age-hardening but rather softens [2,3,7], unlike fcc metals that are hardened primarily by aging rather than by quenching; and (2) vacancy cluster defects, such as prismatic dislocation loops and stacking fault tetrahedra are not usually observed in as-quenched Fe–Al,

* Corresponding author. Present address: Metals and Ceramics Division, Oak Ridge National Laboratory, Oak Ridge, TN 37831-6115, USA.

[1] Printed Wiring Board Div., Process Technology Development Dept., Fujitsu Co., Ltd. 36 Kitaowaribe, Nagano 381, Japan

0921-5093/98/$ - see front matter © 1998 Elsevier Science S.A. All rights reserved.
PII S0921-5093(98)00920-4

as the observable vacancy clusters are called. However, there are a couple of exceptions to the latter. Crimp and Vedula [8] investigated the compressive properties of B2 FeAl single crystals strengthened by excess vacancies at room temperature, and found that many dislocation loops are formed by deformation. Morris et al. [9] observed void formation, likely by vacancy agglomeration. Although the formation of these defects can be attributed to excess vacancies, the strengthening mechanism has not yet been understood.

In order to understand the strengthening mechanism(s), it is required to investigate plastic deformation of vacancy-strengthened Fe–Al in more detail. The purpose of this study is to obtain tensile properties of single crystals strengthened by excess vacancies. After deformation, postmortem deformation microstructures are observed in a transmission electron microscope (TEM), and the strengthening mechanism is discussed.

2. Experimental details

The master Fe–Al alloy ingots were made by arc-melting in an argon atmosphere from 99.99% pure aluminum and iron. Single crystal rods of approx. 25 mm in diameter were grown from the master ingots by the Bridgman technique. Chemical analysis gave three single crystals of compositions, Fe-33, 41 and 44 mol% Al, respectively. Hereafter, the compositions are described as Fe-33Al, Fe-41Al and Fe-44Al throughout this paper. These crystals were homogenized at 1373 K for 48 h in a vacuum, and then slowly cooled to room temperature at the rate of 5×10^{-3} $K \cdot s^{-1}$. Oriented tensile specimens were cut from the homogenized crystals by an electro-discharge machine (EDM). The specimen shape and size are described in Fig. 1a, and the tensile axis is shown in Fig. 1b. A few specimens of the three single crystals were vacuum-sealed in silica tubes, and re-annealed at 1173 K for 1 h, and then fast cooled by taking the silica tubes out of the furnace. A few specimens of the three single crystals were further annealed at 698 K for 100 h in a vacuum to eliminate supersaturated excess vacancies, and then furnace-cooled without controlling the cooling rate. As-homogenized tensile specimens are designated as 'Specimen A', fast cooled ones as 'Specimen B', and fully annealed ones at 698 K as 'Specimen C'. The thermal histories mentioned above are shown schematically in Fig. 2. Before tensile tests, specimen surfaces were mechanically polished and electropolished in a 10% perchloric acid-methanol solution at voltage of 10.5 V and temperature of approx. 248 K.

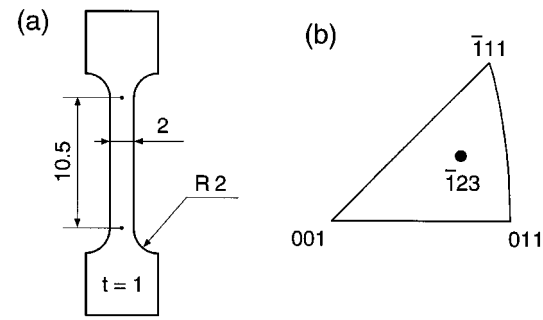

Fig. 1. (a) Shape and size of tensile specimen. The unit is 'mm'. (b) Tensile axis close to [$\bar{1}$23] shown in the standard [001]-[001]-[$\bar{1}$11] unit triangle.

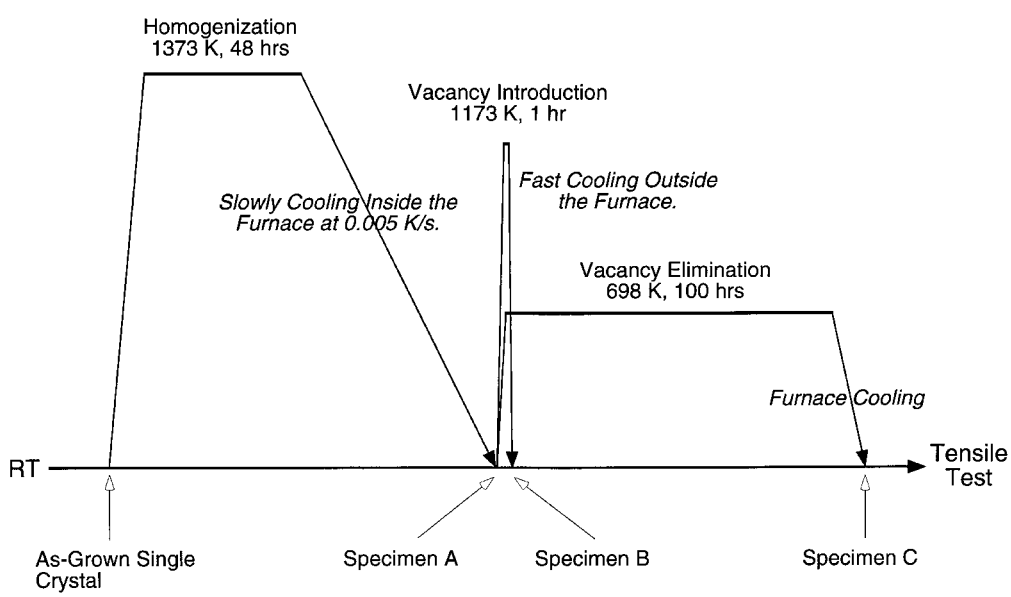

Fig. 2. Schematic diagram of thermal histories of tensile specimens.

Tensile tests were conducted using an Instron 8562-type machine in a vacuum better than 2×10^{-3} Pa at room temperature. All load-displacement data were recorded in two ways with analogue and digital signals. The displacement was measured with an extensometer equipped outside the furnace. An initial strain rate of 1.6×10^{-4} or 1.6×10^{-5} s^{-1} was applied. Some specimens were strained to approx. 4% at 1.6×10^{-4} s^{-1}, and disks parallel to the $(\bar{1}01)$ plane were sectioned from them by EDM. Thin foils for TEM observation were produced by electropolishing these disks in a Struers Tenupol-3 in a 33% nitric acid-methanol solution at 4 V and 248 K. TEM observation was performed in a Hitachi H-8100D electron microscope at 200 kV.

3. Results

Fig. 3 shows resolved shear stress–strain curves of the three specimens deformed at 1.6×10^{-4} s^{-1}. All of the specimens were deformed to failure. The resolved shear stresses and the shear strains are calculated assuming the $(\bar{1}01)[111]$ primary slip system, which is the most reasonable one according to earlier work [8,10,11]. All the as-homogenized and vacancy-eliminated specimens (Specimens A and C) start to work-harden immediately after yielding (i.e. no yield-drop). These work-hardening rates gradually accelerate with strain, and merge into a linear stage (stage II). The plastic flow behavior of fast-cooled specimens (Specimens B) is distinctly different from that of Specimens A and C. The CRSSs are increased by fast cooling even in Fe-33Al. However, elongation is reduced significantly, at higher Al concentrations. It should be noted that Specimens B display serrated flow after a discontinuous yielding followed by distinct work-hardening. In Fe-41 and 44Al, this serrated flow behavior continues until the specimens failed, and is more pronounced at the higher Al concentration, as shown in Fig. 4. It is believed that all these differences in Specimens B are attributed to excess vacancies retained by fast-cooling.

Fig. 5 shows the variation of CRSS at the strain rate of 1.6×10^{-4} s^{-1} with Al concentration. While the CRSSs of Specimens C are slightly lower than those of Specimens A, they are essentially independent of Al concentration. On the other hand, the CRSS of Specimens B shows a strong dependence on Al concentration. The difference between CRSS of Specimen B and others is significant ($\sim$50%) at 33 mol% Al. Moreover, the CRSS is nearly four times higher than that of Specimens A and C at 44 mol% Al. These results are in agreement with the Vickers hardnesses reported in previous papers [1,3–5].

As mentioned above, a linear stage of work-hardening is observed on each s–s curve in Fig. 3 clearly,

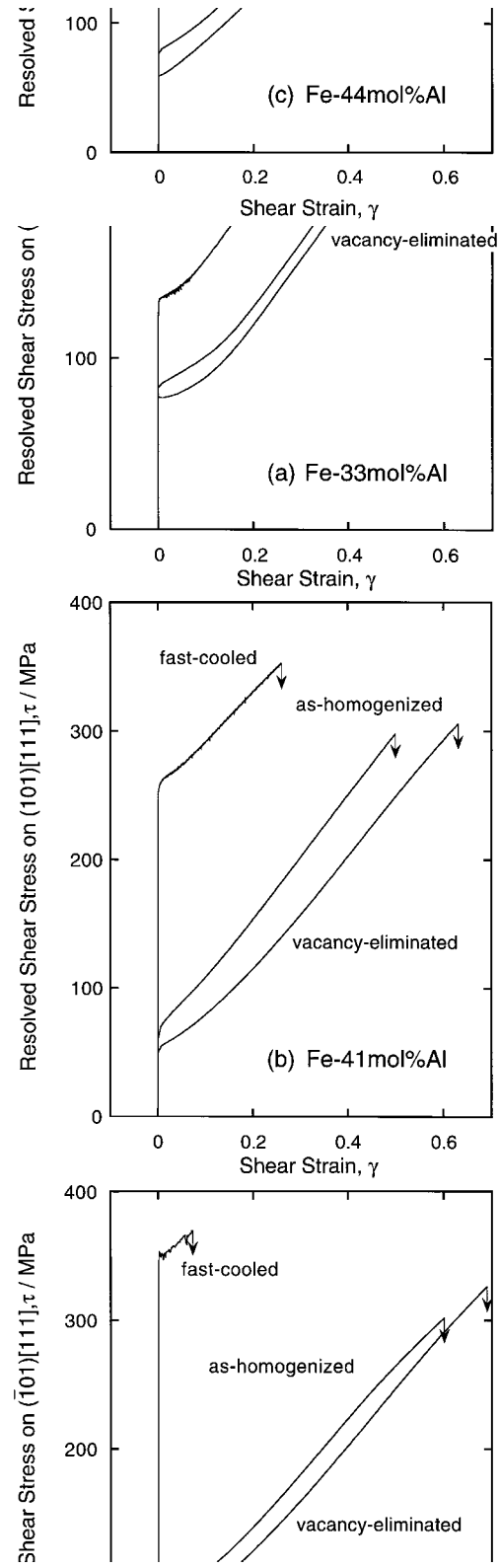

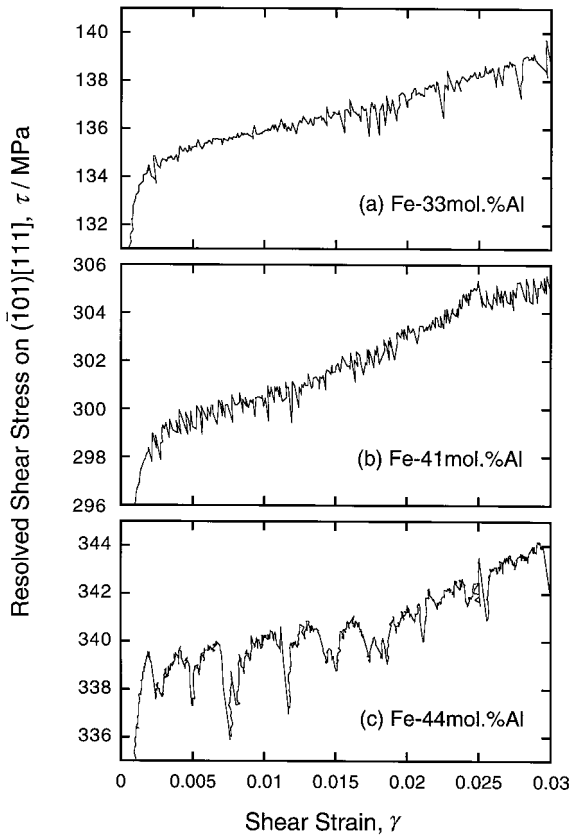

Fig. 4. Serrated flow of fast-cooled tensile specimens. (a) Fe-33 mol% Al; (b) Fe-41 mol% Al; and (c) Fe-44 mol% Al.

even for fast-cooled, serrated ones. The work-hardening rate was analysed at the linear stage for all the s–s curves. Fig. 6 shows the variation of work-hardening rate in stage II against Al concentration, at a strain rate of 1.6×10^{-4} s^{-1}. At 33 mol% Al, the work-hardening rate is almost the same in the three Specimens. In the B2 region, the work-hardening rates of Specimens A and C are also almost the same but higher than Fe-33Al. On the other hand, the work-hardening rate of Specimen B is distinctly lower than the others. In particular, the value of Fe-44Al is smaller than that of Fe-41Al. The decrease in work-hardening rate due to excess vacancies was also reported in the earlier studies that were carried out using single crystals under compression [12,13].

Effects of strain rate on tensile flow properties were also examined. Fig. 7 shows resolved shear stress–strain curves of Specimens A and C of Fe-41Al obtained by strain-rate change tests. The initial nominal strain rate is 1.6×10^{-4} s^{-1}. The downward arrows correspond to a 10-fold decrease of the cross-head speed (i.e. $\dot{\epsilon}=1.6\times10^{-4}\ s^{-1}\rightarrow1.6\times10^{-5}\ s^{-1}$),

Fig. 3. Resolved shear stress–strain curves of Fe–Al subjected to three different heat treatments. (a) Fe-33 mol% Al; (b) Fe-41 mol% Al; and (c) Fe-44 mol% Al.

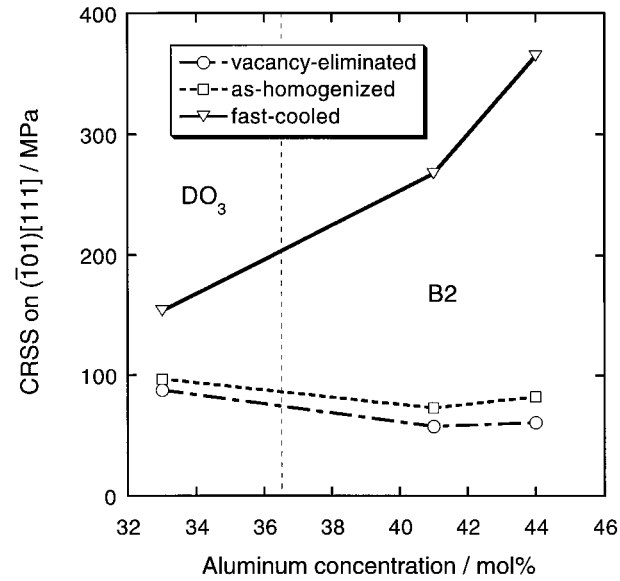

Fig. 5. CRSS against aluminum concentration.

and the upward arrows correspond to a 10-fold increase (i.e. $\dot{\epsilon}=1.6\times10^{-5}\ s^{-1}\rightarrow1.6\times10^{-4}\ s^{-1}$). The dotted curve is the resolved shear stress–strain plot of Specimen C obtained in a normal tensile test without a strain-rate change. When the strain-rate is decreased at the shear strain of 0.05, the flow stress is slightly decreased initially, but it immediately begins to restore itself to give a steady work-hardening. However, by comparing the curve obtained by the strain-rate change test with the dotted curve of Specimen C, it is seen that the incremental rate of increase in flow stress is raised only by the 10-fold decrease of strain-rate. When the strain-rate is increased, the flow

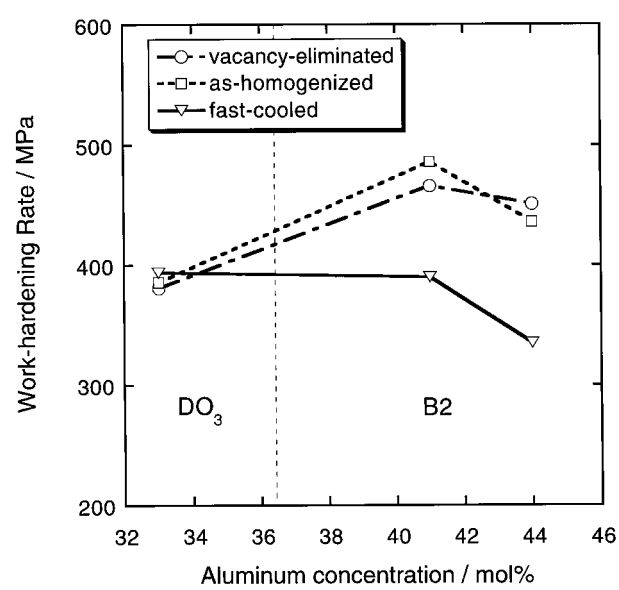

Fig. 6. Work-hardening rate against aluminum concentration.

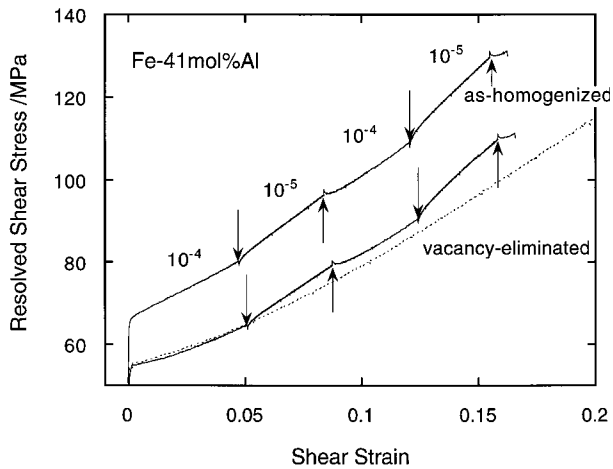

Fig. 7. Highly magnified resolved shear stress–strain curves of Fe-41 mol% Al single crystals obtained by strain-rate change tests. Dotted line shows a standard s–s curve with no strain rate change.

stresses show a transient increase, followed by the same work-hardening rate as of the specimen under the constant strain rate (i.e. $\dot{\epsilon} = 1.6 \times 10^{-4}$ s^{-1} for the dotted curve). These flow stress changes are observed repeatedly every time the strain-rate is altered. As a result, the flow stress of Specimen C gradually becomes higher as the strain increases. The same trends are seen also in Specimen A. This increase in flow stress by the decrease in strain-rate means a negative strain rate dependence of work-hardening rate.

Fig. 8 shows highly magnified resolved shear stress–strain curves of Specimens B of Fe-41 (Fig. 8a) and 44Al (Fig. 8b) obtained by strain-rate change tests. The upward and downward arrows have the same meanings as those in Fig. 7. In Specimens B, the transients in flow stress changes are not evident. Furthermore, no apparent change of serrated flow behavior is detected by strain-rate changes. As in Specimens A and C, a negative strain-rate dependence of work-hardening is found in Specimen B.

Figs. 9 and 10 show deformation microstructures of Specimens A and B of Fe-44Al strained to approx. 4%. The Burgers vectors of dislocations in both the microstructures were identified as $\mathbf{b} = [111]$. The deformation microstructure shown in Fig. 10 is clearly different from that in Fig. 9, where the latter shows no specific predominant dislocation orientations similar to those of slowly-cooled B2 FeAl reported in earlier studies [8,11,14]. In Fig. 10, dislocations are inhomogeneously distributed in bundles, and the dislocation bundles are preferentially oriented along a direction approx. 56° from the [111] direction. In addition, there are numerous nano-size dislocation loops having the Burgers vector parallel to the [111] direction. This inhomogeneous dislocation distribution suggests jerky motion of those dislocations during

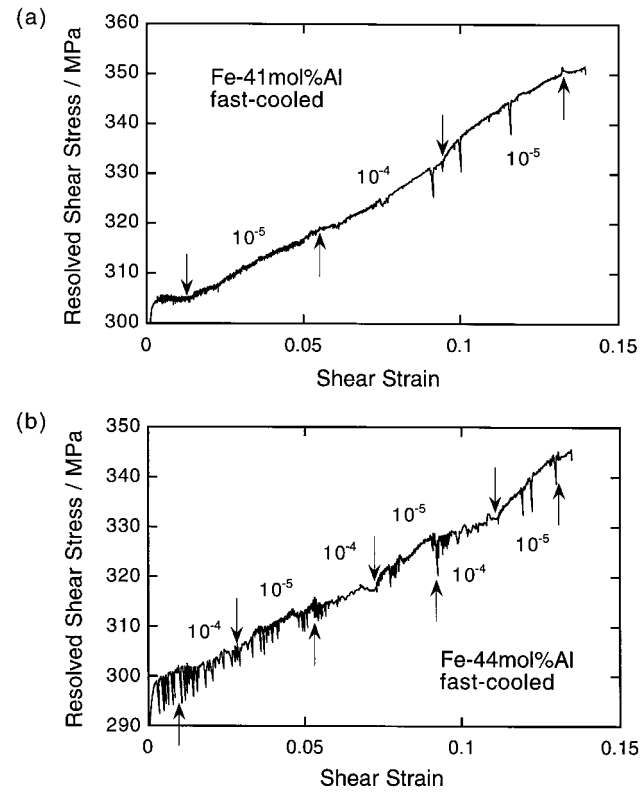

Fig. 8. Highly magnified resolved shear stress–strain curves of fast-cooled (a) Fe-41 mol% Al; and (b) Fe-44 mol% Al obtained through strain-rate change tests.

deformation, which is consistent with the appearance of serrated flow.

4. Discussion

4.1. Yield stress

Using positron lifetime spectroscopy, Würschum et al. [15] determined the effective enthalpy for vacancy formation to be $H_V^F = 1.04$ eV and 0.98 eV for Fe-37Al and Fe-39Al, respectively, and estimated the effective enthalpy for vacancy migration to be $H_V^M = 1.7$ eV for both compositions. The anomalous increase in yield stress of B2 FeAl with increasing temperature is attributed directly to thermal vacancies [16], and a complex of a vacancy on the Fe-site and a neighboring Fe antisite atom on the Al-site is suggested as the defect type responsible for the internal friction peak observed in Fe–Al [17].

In addition, divacancies are expected to play an important role in the interaction of dislocations with vacancies in B2 FeAl [18]. By using the calculated divacancy binding enthalpy [18] of $H_{2V}^B = 0.5$ eV and assuming a divacancy binding entropy of $S_{2V}^B = 1$ k_B, it is estimated from the positron lifetime data [15] that $H_V^F = 0.89$ eV and $S_V^F = 4.2$ k_B, where k_B is the

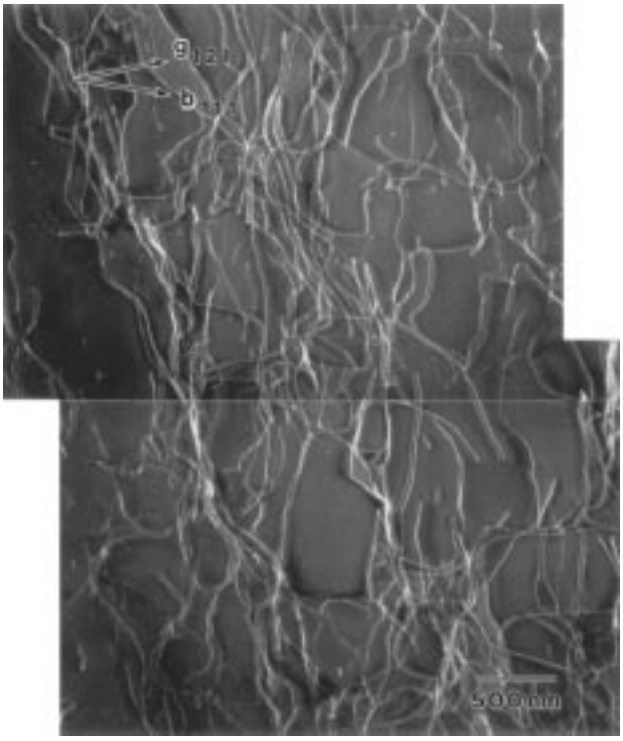

Fig. 9. Deformation microstructure of as-homogenized Fe-44 mol% Al single crystal (Specimen A) strained up to approx. 4%. It was taken in g–3 g weak-beam condition with $g = 121$. The incident beam direction and the normal of the thin foil plane is almost parallel to the $[\bar{1}01]$ direction.

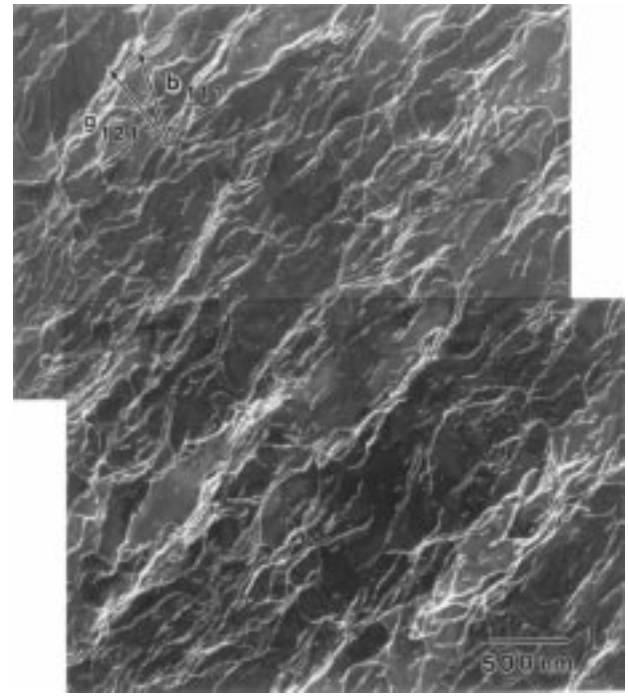

Fig. 10. Deformation microstructure of fast-cooled Fe-44 mol% Al single crystal (Specimen B) strained up to approx. 4%. It was taken in g–3 g weak-beam condition with $g = 121$. The incident beam direction and the normal of the thin foil plane is almost parallel to the $[\bar{1}01]$ direction.

Boltzmann constant. These are slightly lower than those values mentioned in the preceding paragraph, which do not take divacancies into account [15]. Using the above values, equilibrium mono-vacancy concentration, c_V, defined as n_V/N, is given by [19],

$$c_V = \exp\left(\frac{S_V^F}{k_B}\right)\exp\left(-\frac{H_V^F}{k_B T}\right) \tag{1}$$

where n_V is the number of mono-vacancies, N the total number of lattice sites, and T the absolute temperature. Equilibrium divacancy concentration, c_{2V} ($\equiv n_{2V}/N$, n_{2V}; the number of divacancies), can be estimated by the following [19],

$$c_{2V} = g \cdot c_V^2 \cdot \exp\left(\frac{H_{2V}^B - TS_{2V}^B}{k_B T}\right) \tag{2}$$

where g is a divacancy configuration factor. In disordered alloys, $g = z/2$, where z is the coordination number of nearest neighbors. In B2 FeAl, thermal divacancies are formed between next-nearest neighbor sites [18,20,21], thus $z = 6$ is adopted. Consequently, using Eq. (1) and (2), the equilibrium concentration values are determined as: $c_V \approx 10^{-14}$ for mono-vacancy and $c_{2V} \approx 10^{-19}$ for divacancy at room temperature, and $c_V \approx 0.01$ and $c_{2V} \approx 0.016$ at 1173 K are estimated. These show that the equilibrium concentration of divacancy is higher than that of mono-vacancy at high temperatures ($\geq$ 1073 K).

In B2 structure, the number of lattice sites in the unit volume, N_0, is $2/a^3$ ($= 6\sqrt{3}/b^3$), thus the number of mono- or divacancies in the unit volume is $2c_{V\text{ or }2V}/a^3$ ($= 6\sqrt{3}\,c_{V\text{ or }2V}/b^3$), where a is the lattice constant, b the length of the Burgers vector. Considering the $(110)[\bar{1}11]$ slip, since the interplanar spacing of the (110) plane is $a/\sqrt{2}$, the area of the (110) plane in the unit volume is $\sqrt{2}/a$. The total number of mono- and divacancies in the unit volume is $2c/a^3$, where $c = c_V + c_{2V}$. Thus, neglecting the configuration and orientation of divacancies, the vacancy concentration on the (110) plane is $\sqrt{2}\,c/a^2$ ($= 3\sqrt{2}\,c/b^2$), and the mean distance between vacancies (or divacancies) on the (110) plane, $\bar{l}_0$, is

$$\bar{l}_0 = a/\sqrt{c\sqrt{2}}\left(= b/\sqrt{3c\sqrt{2}}\right) \tag{3}$$

The critical shear stress required for a dislocation to break away from two obstacles was represented by Fleischer and Hibbard [22] and Friedel [23] as follows:

$$\tau = \frac{\mu b}{\bar{l}_0}\left(\sin\frac{\theta_c}{2}\right)^{3/2} \tag{4}$$

where μ is the shear modulus, and θ_c the critical angle for break-away from pinning points. Using Eqs. (3) and (4) is written as

$$\tau \cong 2\mu\left(\sin\frac{\theta_c}{2}\right)^{3/2} c^{1/2} \tag{5}$$

If the break-away stress given by Eq. (5) is high enough, the stress estimated by Eq. (5) gives the CRSS for B2 FeAl. Eq. (5) shows that the CRSS is proportional to the square-root of supersaturated vacancy (or divacancy) concentration. This relationship is consistent with that of hardness reported by Pike et al. [4,5] and the vacancy hardening model at elevated temperatures reported by George and Baker [24].

The experimental results on the CRSSs or yield stresses shown in Figs. 3 and 5 are discussed with the aid of Fig. 11 ($\mu = 64.8$ GPa [25,26]), which shows the break-away stress from the equilibrium concentration of mono- and divacancies as a function of temperature. If one assumes the critical angle for mono-vacancies to be $\theta_c^V = 5°$, and the pinning force of divacancies is twice that of mono-vacancies, i.e. $F_{2V} = 2F_V$, the critical angle for divacancies is estimated to be $\theta_c^{2V} \approx 10°$. Taking a hypothetical case of excess divacancies at room temperature, quenched-in from 1073 K by an 'infinitely fast' cooling rate, to represent the fast-cooled Specimen B from 1173 K, the CRSS due to divacancies is estimated to be approx. 230 MPa. This value is in fair agreement with the experimental value interpolated at Fe-39Al of the B2 phase in Fig. 5. In the meantime, the CRSS due to mono-vacancies at 1073 K is 78 MPa. Although the concentration of mono-vacancies ($c_V \approx 4.4 \times 10^{-3}$) is almost the same as that of divacancies ($c_{2V} \approx 4.8 \times 10^{-3}$) at the temperature, breaking away from mono-vacancies is not the rate controlling process in this case. The increase in the CRSS of Specimen B with increasing Al concentration (Fig. 5) is consistent with the decreasing trend of vacancy formation enthalpy found with increasing Al content [15,27].

4.2. Dislocation microstructure

The apparent differences of the dislocation microstructure in the fast-cooled Fe-44Al (Fig. 10) from that in as-homogenized one (Fig. 9) are twofold: (1) the cellar structure formation along a direction approx. 56° from the [111] slip direction; and (2) the formation and distribution of numerous small loops. These differences in dislocation structures result from the excess vacancy distribution in the fast-cooled specimen. The formation of dislocation loops suggests direct-contact interaction of glide dislocations with excess vacancies, as contrasted to an indirect interaction by creating a 'vacancy atmosphere' around dislocation. A direct evidence suggesting the direct-contact interaction of dislocations and vacancies was reported earlier [12]. Development of the cellular microstructure (Fig. 10) may be related to jog–jog interactions resulting from the direct-contact interaction of dislocations with vacancies. An analysis of elastic climb force on non-screw dislocations based on the dislocation line tension is under way, and the results will be reported elsewhere.

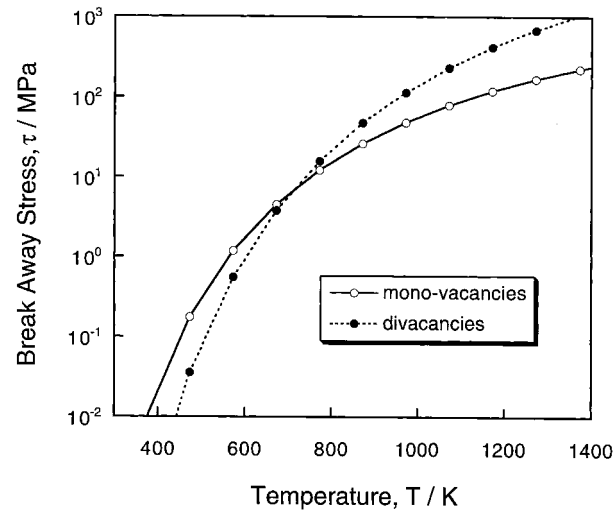

Fig. 11. Break away stress from the equilibrium concentration of mono- and divacancies as a function of temperature.

Vacancies are presumably immobile in the bulk of Fe–Al at room temperature. Thus, they would not be able to form any atmosphere like the Cottrell atmosphere around dislocations. Furthermore, if they could not migrate along dislocation core, vacancies would behave simply like solute atoms. Although they might hinder dislocation motion during this process, vacancies and small vacancy clusters are left behind the dislocation movement after the direct-contact interaction without any change by means of the dislocation as the source as well as the sink for vacancies and vacancy clusters. The Orwan loop formation mechanism is quite unlikely to occur in this case.

On the other hand, if vacancies could migrate along the dislocation core by a pipe-diffusion mechanism, they can be accumulated at the jog and change the dislocation configuration to form super-jogs, dipoles and so on. In order to by-pass these pinning points, dislocations have to pinch them off, consequently loops may be left behind. These pinning points would exert stronger glide resistance to dislocations than mono-vacancies or divacancies. In other words, the distribution of the loops in the dislocation microstructure strongly suggest the existence of some pinning points stronger than mono-vacancy.

4.2.1. Work-hardening rate

The effect of thermal history on work-hardening

rate is obvious in the B2 region (Fig. 6). As mentioned in the above section, a glide dislocation may act as the sinks for vacancies. This means that non-equilibrium, supersaturated vacancies are absorbed by glide dislocations. The increase in strain results in the reduction of excess vacancy concentration by the process that dislocations sweep them out. This could be the reason why the work-hardening rate is lower for the fast-cooled specimens than for the others in the B2 region (Fig. 6). The strong Al concentration dependence of CRSS of the fast-cooled specimens (Fig. 5) indicates that the excess vacancy concentration is higher for the higher Al content, because the CRSS of as-homogenized and vacancy-eliminated specimens is almost independent of Al concentration in the test range. Since the frequency of dislocations making direct-contact with vacancies is higher for the higher vacancy concentration, i.e. for the higher Al concentration in this case, the reduction rate of excess vacancy concentration is faster for the higher Al concentration. This may be the reason why the work-hardening rate of the fast-cooled specimen becomes lower as Al concentration increases in the B2 region (Fig. 6). In the $D0_3$ region, there is essentially no change of work-hardening rate by the thermal history. In addition, the serrated flow disappears at the strain of approx. 0.1 (Fig. 3a). These results indicate that excess vacancies are exhausted by the direct-contact interaction process mentioned above.

The negative strain-rate dependence of work-hardening rate (Figs. 7 and 8) is a very interesting phenomenon, but the mechanism for it is not understood. This anomalous phenomenon is observed in the serrated σ–ϵ curves of the fast-cooled Fe-41 and 44Al (Fig. 8), hinting that it may be attributable to excess vacancies. However, since this is also observed clearly in the as-homogenized and vacancy-eliminated specimens (Fig. 7), it is suggested that this anomalous strain-rate sensitivity of work-hardening rate may be one of the intrinsic properties of B2 FeAl.

5. Conclusions

In this work, the effect of excess vacancies on the room temperature tensile properties of Fe-33, 41 and 44 mol% Al was investigated using single crystals.

1. Significant excess vacancy strengthening was detected over the aluminum composition examined, even in Fe-33 mol% Al. Due to the excess vacancy strengthening, CRSS is increased drastically and elongation is decreased.
2. Dislocation motion obstructed by excess vacancies is interpreted by the break-away process. In fast-cooled specimen, in which the supersaturation of divacancies is comparable to that of mono-vacancies, dislocation–divacancies interaction plays an important role in the strengthening mechanism.
3. The iron aluminides strengthened by excess vacancies exhibit serrated flow during work hardening. In B2 FeAl, work hardening rate is lowered by excess vacancies.
4. Dislocations microstructure in Fe-44 mol% Al were arranged inhomogeneously in the form of bundle structures. Mixed character is predominant in this microstructure, which is in the unstable range of the dislocation line orientation estimated by the anisotropic line-tension calculation.

Acknowledgements

The authors thank Dr J. H. Schneibel and Dr E. P. George for reviewing this paper. This research was sponsored by the program of Japan Society for the Promotion of Science Postdoctoral Fellowships for Research Abroad, and in part by the Division of Materials Sciences, US Department of Energy, under Contract No. DE-AC05-96OR22464 with Lockheed Martin Energy Research Corp.

References

[1] P. Nagpal, I. Baker, Metall. Trans. A 21 (1990) 2281.
[2] J. Rieu, C. Goux, Mem. Sci. Rev. Metall. 65 (1969) 869.
[3] D. Weber, M. Meurtin, D. Paris, A. Fourdeux, P. Lesbats, J. Phys. C7 38 (1997) 332.
[4] Y.A. Chang, L.M. Pike, C.T. Liu, A.R. Bilbrey, D.S. Stone, Intermetallics 1 (1993) 107.
[5] L.M. Pike, Y.A. Chang, C.T. Liu, Acta Mater. 45 (1997) 3709.
[6] H. Kimura, R. Maddin, in: Quenching Hardening in Metals, North-Holland Publishing Company, Amsterdam/London, 1971.
[7] J.P. Rivière, H. Zonon, J. Grilhé, Phys. Stat. Sol. (a) 16 (1973) 545.
[8] M.A. Crimp, K. Vedula, Philos. Mag. A 63 (1991) 559.
[9] D.G. Morris, J.C. Joye, M. Leboeuf, Philos. Mag. A 69 (1994) 961.
[10] K. Yoshimi, S. Hanada, M.H. Yoo, Acta Metall. Mater. 43 (1995) 4141.
[11] K. Yoshimi, S. Hanada, M.H. Yoo, Intermetallics 4 (1996) 159.
[12] K. Yoshimi, S. Hanada, M.H. Yoo, Intermetallics 4 (1996) S159.
[13] K. Yoshimi, S. Hanada, J. Met. 49 (1997) 46.
[14] K. Yoshimi, S. Hanada, in: R. Darolia, J.J. Lewandowski, C.T. Liu, P.L. Martin, D.B. Miracle, M.V. Nathal (Eds.), Structure Intermetallics, TMS Publications, Warrendale, PA, 1993, p. 475.
[15] R. Würschum, C. Grupp, H.-E. Schaefer, Phys. Rev. Lett. 75 (1995) 97.
[16] R. Carleton, E.P. George, R.H. Zee, Intermetallics 3 (1995) 433.
[17] H.-E. Schaefer, B. Damson, M. Weller, E. Arzt, E.P. George, Phys. Stat. Sol. (a) 160 (1997) 531.

[18] C.L. Fu, Y.-Y. Ye, M.H. Yoo, K.M. Ho, Phys. Rev. B 48 (1993) 6712.
[19] A.C. Damask, G.J. Dienes, in: Point Defects in Metals, Gordon and Breach, Science Publishers, New York, 1963.
[20] D. Paris, P. Lesbats, J. Levy, Scr. Metall. 9 (1975) 1373.
[21] R. Krachler, H. Ipser, B. Sepiol, G. Vogel, Intermetallics 3 (1995) 83.
[22] R.L. Fleischer, W.R. Hibbard, Jr., in: The Relation between the Structure and Mechanical Properties of Metals, H. M. S. O., London, 1963, p. 261.
[23] J. Friedel, in: G. Thomas, J. Washburn (Eds.), Electron Microscopy and Strength of Crystals, Interscience, New York, 1963, p. 605.
[24] E.P. George, I. Baker, Phil. Mag. A, in press.
[25] H.J. Leamy, E.D. Gibson, F.X. Kayser, Acta Metall. 15 (1967) 1827.
[26] M.J. Marcinkowski, G. Lakso, J. Appl. Phys. 38 (1967) 2124.
[27] T. Haraguchi, M. Kogachi, in: M.V. Nathal, R. Darolia, C.T. Liu, P.L. Martin, D.B. Miracle, R. Wagner, M. Yamaguchi (Eds.), Structure Intermetallics 1997, TMS Publications, Warrendale, PA, 1997, p. 769.